Abd El-Latif, Mohamed Y.; Yossef, Mostafa; Chen, An; Elsayad, Mohamed

Behavior of stressed skin corrugated sheet under hydrostatic loads

Published in:
Case Studies in Construction Materials

DOI:
10.1016/j.cscm.2024.e03343

Published: 01/07/2024

Document Version
Publisher's PDF, also known as Version of record

Case Studies in Construction Materials 20 (2024) e03343

Contents lists available at ScienceDirect

Case Studies in Construction Materials

journal homepage: www.elsevier.com/locate/cscm

Behavior of stressed skin corrugated sheet under hydrostatic loads

Mohamed Y. Abd El-Latif[a,*], Mostafa Yossef[b,d,**], An Chen[c], Mohamed Elsayad[d]

[a] Dept. of Structural Engineering, Ain Shams University, Cairo, Egypt
[b] Dept. of Civil Engineering, Aalto University, Espoo, Finland
[c] School of Civil Engineering, Beijing Jiaotong University, Beijing, China
[d] Dept. of Construction and Building Engineering, Arab Academy for Science, Technology and Maritime Transport, Cairo, Egypt

A R T I C L E I N F O

Keywords:
Thin-walled steel
Water tanks
Corrugated plates
Diaphragm action
Stressed skin sheet

A B S T R A C T

Water storage in buildings is an integral part of water supply, which can be used for firefighting and drinking. It can be divided into three categories: elevated, rooftop, and underground water tanks. This paper presents a novel water storage system consisting of thin-walled corrugated steel sheets, which can be installed in a multi-story building on any floor. Compared with a reinforced concrete tank, the integrated steel water tank can be fabricated and installed much faster and store freshwater more easily. To develop the system, a finite element model is developed, which is validated using the on-site measurements. Next, the model is used to conduct a parametric study to evaluate the effects of boundary conditions, panel depth, sheet thickness, trough-to-crest width ratio, and corrugation angle on the behavior of integrated steel water tanks. The model is further used to evaluate the water tank subjected to lateral diaphragm loads and report the tank stiffness under combined loads. Finally, an implementation guide for the steel tank is presented, showing the supporting system, vacuum and magnetic handling of steel panels, robotic welding techniques, and delivery. It can be concluded that the paneled steel tank can be an efficient solution for water storage inside buildings.

1. Introduction

Corrugation can increase the stiffness of steel sheets. As a result, corrugated sheets have been used as building applications, including shadings, beam webs, floor diaphragms, and recently in shear walls [1–3]; and non-building applications, including load-bearing element in silos, sheet-pile walls, and transport containers [4]. They can also be used as water storage system in buildings. Typically, buildings are subjected to horizontal and vertical loads, such as dead, live, wind, and seismic loads. However, special considerations are required when the building contains a water storage system within one of its floors. These considerations can vary depending on the location of the building, the water tank level floor, and the overall stiffness of the building. For example, if the building exists in an active seismic area, the water tank located on the roof can act as a liquid damper [5].

* Correspondence to: Ain Shams University.
** Correspondence to: Arab Academy for Science, Technology and Maritime Transport.
E-mail addresses: Mohamed.youssef@eng.asu.edu.eg (M.Y. Abd El-Latif), myossef@aast.edu (M. Yossef), mohamed_elsayaad@aast.edu (M. Elsayad).

https://doi.org/10.1016/j.cscm.2024.e03343
Received 16 September 2023; Received in revised form 27 March 2024; Accepted 26 May 2024
Available online 28 May 2024
2214-5095/

1.1. Water tanks

Climate change has increased drought in large parts of the earth, where water storage become an essential need. This need can be addressed by repurposing some of the building floors for water storage. The stored water can be used for multiple purposes, including drinking, utilities, and firefighting [6–8]. Different storage systems can be used to supply water for residential areas, including elevated rooftops and underground water tanks [9]. Elevated tanks, built as separate structures, are often constructed using rounded or squared shapes [10,11]. Rooftop water tanks are built as a secondary option to provide water demand for the residents of some buildings and act as solar water collectors [12,13]. Another advantage of storing the water on the top of the building is that it can provide adequate water pressure heads for residents. Underground water tanks provide a more accessible way in terms of design and practice. However, it consumes additional energy for water pumps to lift water to the residents, depending on the elevation of the floor. It also needs to be protected against soil severity [14].

Several materials can be used for tanks, including steel, concrete, and fiberglass. Steel tanks are considered more advantageous than concrete water tanks in buildings for several reasons:

1) Increasing the construction speed of the buildings, as concrete tank, which requires concrete formwork, steel reinforcement, casting, setting and curing of concrete, and dismantling of formwork, will delay the construction of upper floors.
2) Saving building weight, hence decreasing the seismic effect, as the self-weight of the steel tank is considerably less than that of the concrete tank. Consequently, it will save in the required design dimensions of supporting elements such as columns, walls, and foundations.

Steel storage tanks are also widely used in transportation and temporary storage in remote areas, including Frac tanks, mud tanks, and solid waste tanks, which consist of outer steel corrugated sheets and inner multiple perforated steel sheets to limit the liquid sloshing during transportation. Such tanks mainly transport liquids and are rarely used in buildings [15,16].

The standardization process of steel tank design started in the early 1930s for riveted tanks, which progressed into the welded design. The latest standards for welded steel tanks are API 650 – Welded Steel Tanks for Oil Storage in the US and EN14015 in Europe. Other standards for welded steel tanks to store water include ANSI/AWWA D100, published by the American Water Works Association (AWWA), which also provides loads for seismic design [17,18].

Standards characterize the tanks according to their pressure. For example, EN14015 divides the design pressure into four categories: up to 10, 25, 60, and 500 mbar, respectively. Water tanks belong to the first category of non-pressure (up to 10 mbar). Most of the aforementioned codes focus on regular shapes of steel tanks, such as circular shell tanks. Circular shell tanks are commonly used in petrochemical plants for liquid storage and elevated water tanks. They are suitable for large tanks with a diameter of up to 100 m, as their height is divided into multiple plates, each with a different steel thickness. Since this design avoids using the same thickness for the steel tank wall, it can reduce the weight and cost of the overall system [19,20]. While circular tanks are convenient for self-standing tanks, they cannot be used for water storage in buildings due to their irregular shape [21]. Therefore, single-skin corrugated sheets act as an excellent option to provide water storage for buildings, since they can be adapted to the floor layout while providing lateral support through diaphragm action.

Steel corrugated panel's structural behavior was studied under various loading conditions, emphasizing its advantages in seismic resilience [22–26], buckling capacity, and shear strength [23,27,28]. Innovations in design and analysis methods included double corrugated shear walls, multi-stiffened configurations, optimization in diverse applications such as deep-sea structures, tunnel supports [29], and sandwich panels for lateral loads [30]. These contributions are pivotal in advancing the application of corrugated steel in engineering, highlighting its benefits in improving structural performance and safety in both conventional and novel engineering solutions.

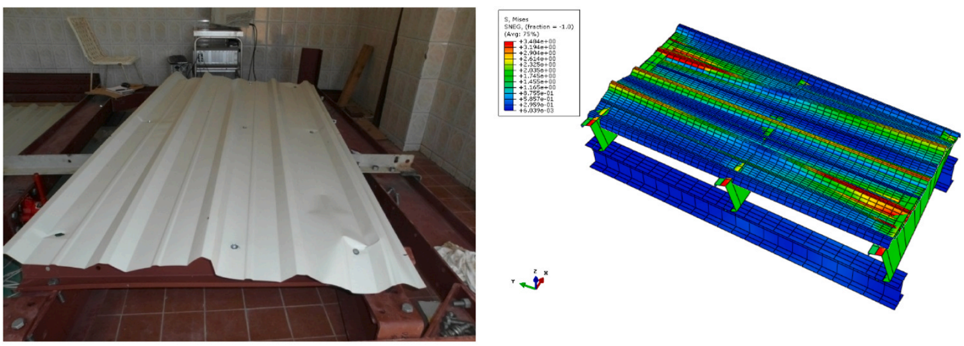

(a) (b)

Fig. 1. Deformed shape for panel with 0.5 mm sheet thick, two fasteners, and C200 purlin cross-section, (a) experimental testing, (b) FE model [32].

1.2. Diaphragm action of stressed skin sheets

Stressed skin corrugated sheets have been widely used as non-bearing elements, such as roof and wall panels for steel portal frames. The diaphragm action of single-skin sheets was first introduced by Bryan [31], with the goal of multiusing the sheets in bearing elements and reducing the use of the bracings. Since then, the diaphragm action of single-skin sheets has progressed to include riveted and welded designs, and linear and nonlinear behaviors. Yossef conducted experimental tests to study the effect of purlin cross-section, panel thickness, number of fasteners, and panel aspect ratio [32]. Nagy et al. [4] studied the rafter-purlin connection's flexibility and its influence on the corrugated sheet. Recently, Davies published a comprehensive review of the stressed skin sheets theory, highlighting the safety concerns for big sheds [33].

1.3. Objective

This paper presents a novel building-integrated thin-walled irregular structural steel tank, which is built on the floor and follows the architectural layout shape of the floor. Unlike traditional circular tanks, the relatively limited height of the floor requires further study for the proposed system. The steel tank is formed from single-skin corrugated sheets that aim to provide diaphragm action to resist existing hydrostatic pressure. To this end, a Finite Element (FE) model is constructed based on prior research on the diaphragm action of corrugated sheets shown in Fig. 1 [32,34]. A parametric study is conducted using the FE model, based on which a tank with optimized dimensions is proposed. Finally, a full-scale steel tank is constructed based on the FE results, and on-site deflection measurements are recorded, confirming the accuracy of the FE model.

2. Tank system

To develop a tank that can resist hydrostatic pressure and diaphragm action, typical failure modes of corrugated sheets subjected to diaphragm action need to be studied to avoid water leakage or catastrophic failures. To avoid these failures, the following assumptions are taken into consideration:

1. Welding will be used in all connections that are subjected to water to avoid water leakage through the fasteners.
2. Thicker bendable sheets will be used to avoid sheet deformation and failure due to combined compression and bending.
3. Removing support elements such as purlins and replacing them with stiffened angles and end plates to avoid all end failures, including sheet warping and purlin failures.

The proposed tank system consists of corrugated wall panels that have the same thickness along the height. The wall panel consists of several corrugations, has specific width for transportation purposes, and is welded to the neighboring panel. The main loads on tank walls are lateral water pressure and transverse displacement due to water sloshing or wind loads. The vertical load is typically neglected through the proposed configuration. Fig. 2 shows the inside and outside of the tank panel wall.

3. Numerical study

An FE model is constructed using commercial software ABAQUS. The previous FE model shown in Fig. 1 is improved to mitigate risks from failures that occur due to hydrostatic pressure and diaphragm action. The improved FE model consists of a corrugated sheet, cap plate, side plates, anchor bolts, and angles with stiffeners. The corrugated sheet consists of 3 pitches (i.e., four crests and five troughs) with a pitch dimension of 470 mm, as shown in Fig. 3. The pitch dimension can be measured from the middle of the crest to the following crest. The assembly of the corrugated sheet, angles, and plates is defined as a panel in this paper for easier referencing.

The FE model is first studied at two stages. The first stage is applying the panel's weight and hydrostatic pressure. The deflection results from the FE model are validated using on-site measurement, as will be discussed in the next section. Parameters, including

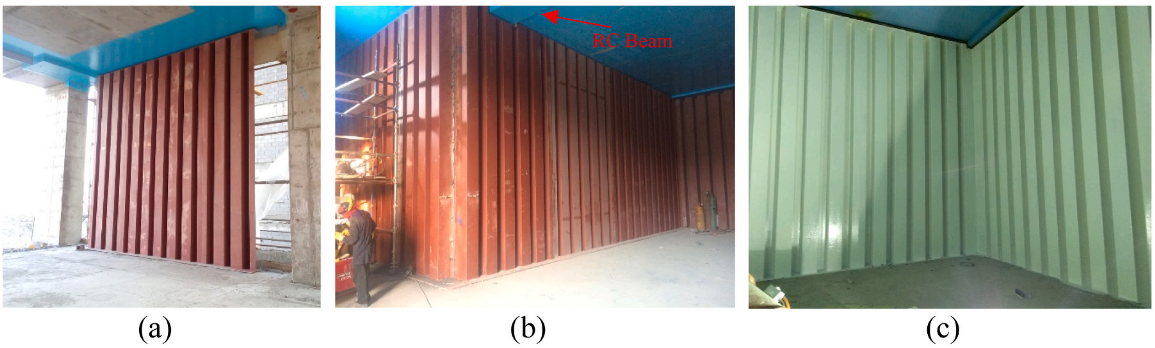

Fig. 2. Site photos for the steel tank wall panels (a) two aligned panels (b) multi-aligned panels (c) panels from inside tank after painting.

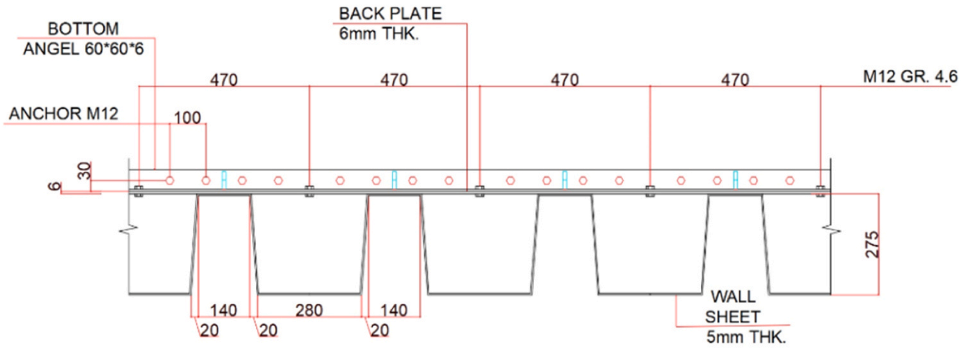

Fig. 3. Dimensions of the bottom part of the corrugated panel with support location.

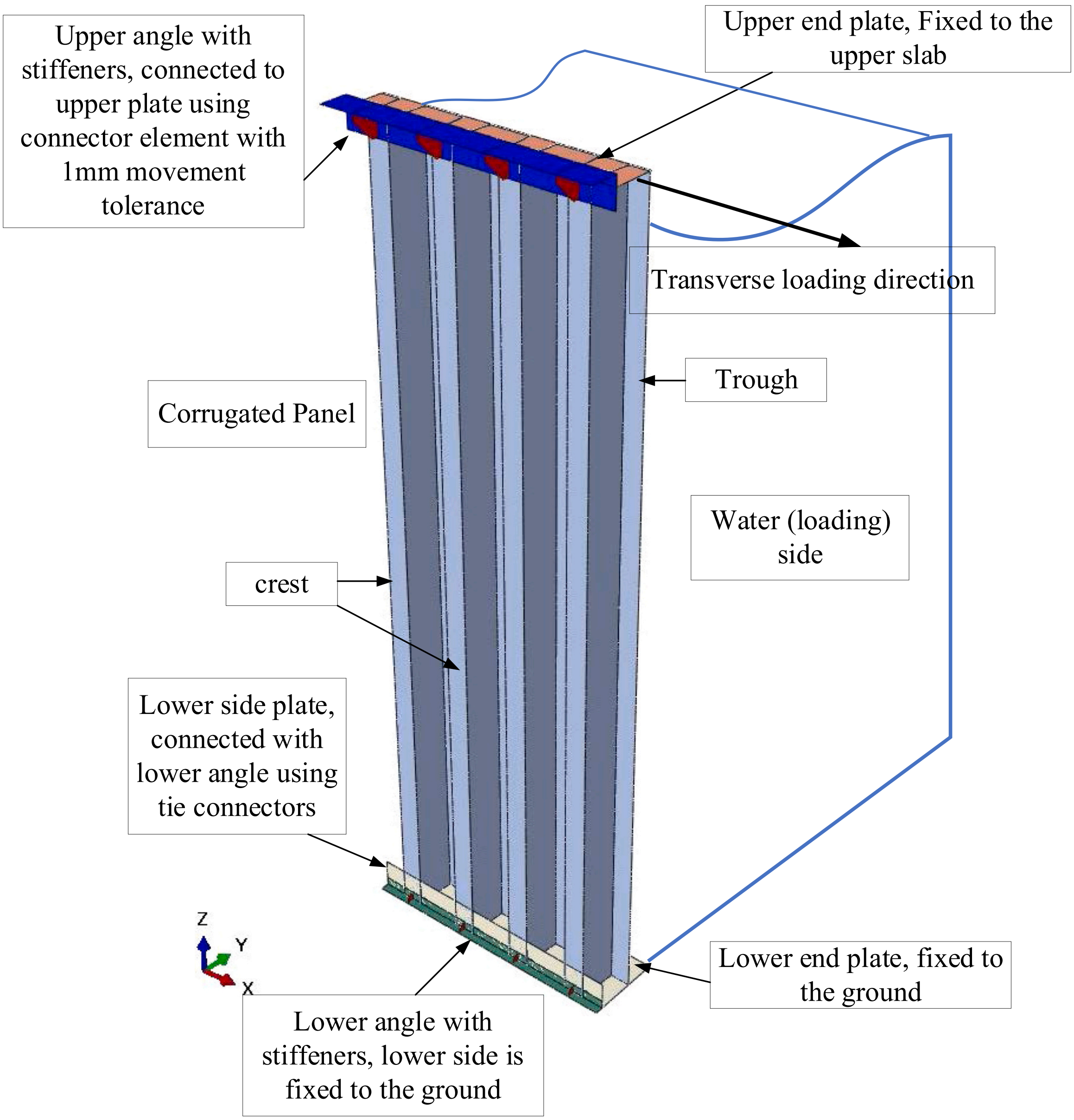

Fig. 4. Sketch of tank partition showing different components.

boundary conditions, corrugated depth, sheet thickness, trough-to-crest width ratio, and corrugation angle, are varied to evaluate the best combination for hydrostatic pressure. The second stage is applying a transverse displacement at various water levels, evaluating their effects on the maximum stress (Fig. 4).

3.1. Material properties

High-strength steel grade (S355) is adopted, with Young's modulus of 210,000 MPa, yield strength of 355 MPa, poison's ratio of 0.3, and density of 7750 kg/cm^3. The stress-strain curve is shown in Fig. 5 [35]. To be used in the FE model, the engineering stress and strain are converted into true stress and strain, as shown in Fig. 5 [36].

3.2. Geometry

The panel is divided into several parts with different dimensions. All parts are defined as shell elements with an element type of S3R, which is a three-nodal element with reduced integration that can be used for different shapes, providing the ability to model irregular geometry and exhibit nonlinear element behavior.

A convergence study is conducted to determine the mesh size. The panel's mesh size varies from 5 mm to 100 mm, while the load is kept constant according to the next section. The loading system is performed with ten sub-steps to simulate the gradual change. Fig. 6 shows the convergence performance of the deflection profile along the panel height at different mesh sizes. The deflection varies with different mesh sizes until 20 mm, where the deflection difference is negligible compared to the 5 mm while the computational time decreases by more than 300 %. Therefore, a mesh size of 20 mm is selected.

3.3. Loads

The loads consist of the panel's own weight, hydrostatic pressure, and transverse displacement. The first stage contains both the panel's own weight and hydrostatic pressure. The hydrostatic pressure (P) is calculated as follows:

$$P = \rho \cdot g \cdot h = 1000\frac{kg}{m^3}\cdot 9.807\frac{m}{s}\cdot 5m = 0.049MPa \tag{1}$$

where ρ is water density, g is the gravitational acceleration, and h is the maximum water height in the static loading case at about 90 % of the total floor height, i.e., 5 m. The hydrostatic pressure (P) is created by defining zero-pressure and hydrostatic pressure locations.

The second stage contains the transverse displacement acting in the x-axis direction to study the diaphragm action of the panel. The upper plate is divided into several face partitions to model the exact behavior of the panel. Partitions are divided according to the location of the connection between the upper side plate and the upper angle to contain one pitch (from the middle of the trough width to the middle of the following trough width). Each partition is connected to a reference point in its center using a kinematic coupling constraint. All reference points are then grouped into a set with which the transverse displacement is applied in the x-direction.

3.4. Boundary conditions

To avoid over-constraining, the lower angle's bottom and upper angle's top surfaces are fixed, while the upper end, lower end plate, and lower side plates are attached to the corrugated sheet as one assembly. Lower plate and angle are fixed to the ground as shown in Fig. 4, and tied to each other at 200 mm height to represent the existing welding between the lower plate and angle, allowing flexible rotation of the panel around the x-axis while restraining its movement in the x-axis to provide diaphragm action. Furthermore, the upper side plate and the upper angle are attached at fastener locations. The fasteners are assumed to have a 1 mm movement tolerance in the z-direction to reduce the axial stresses in the sheet due to the transverse movement. This is achieved by adopting a connector type "stop," which allows the 1 mm tolerance, after which the model is restrained in the assigned direction. The corrugated sheet sides are restrained against rotation around y and z directions to simulate adjacent panels.

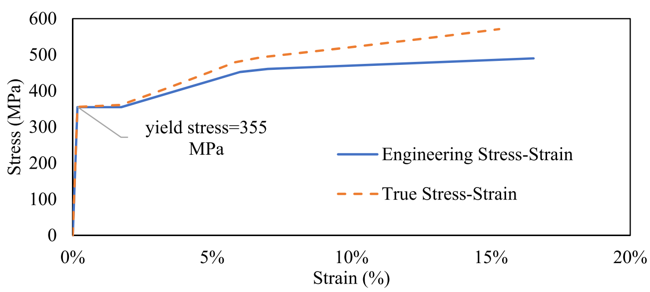

Fig. 5. Stress-Strain Curve for Steel grade S355.

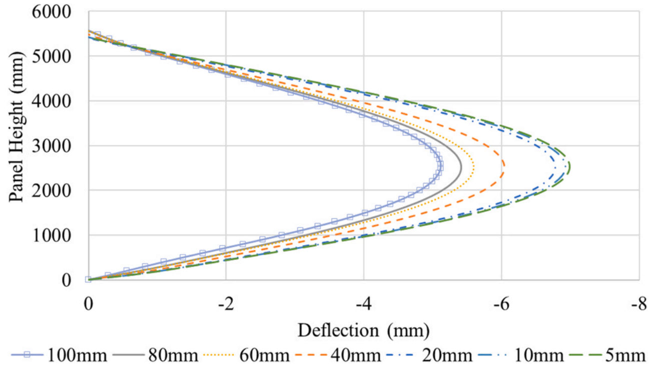

Fig. 6. Convergence Study for different mesh sizes at maximum deflection.

3.5. Validation

Thin-walled corrugated steel tank is constructed, with details shown in Section 4. Validation of the FE model on corrugated sheet was carried out in a previous study, as shown in Fig. 1. In this paper, validation of the FE model on the tank subjected to hydrostatic pressure is performed using a non-destructive test. Five dial gages are placed on the steel tank wall from the outside, as shown in Fig. 7. On-site readings are taken at three different water levels, i.e., 2.86 m, 3.6 m, and 5 m. Fig. 8 shows a good agreement between the FE results and the on-site displacement measurements, which validates the FE model.

3.6. Hydrostatic loading

The previous model geometry is used as a benchmark, with 275 mm corrugated panel depth, 5 mm thickness, 86 pitch angle, and 280 mm trough width. The water level is set to be the maximum possible height, which is 5000 mm, and the corresponding load is 0.049 MPa, as calculated using Eq. (1).

3.6.1. Boundary conditions

Boundary conditions (BCs) are varied by removing all the end plates for the sake of the study. BCs have a significant influence on the displacement of the panel, as shown in Fig. 9. Each case is referred to as Bottom BC – Top BC. The fixed-hinged BC has the lowest displacement (3.58 mm), followed by hinged-hinged (5.19 mm) and hinged-roller (7.85 mm) BCs. It is worth noting that the boundary conditions provided in Section 3.3 match the hinged-roller case, validating the concept of free rotation while providing support in the *x*-direction.

3.6.2. Corrugated depth

The effect of corrugated depth is studied from 50 mm to 300 mm with 50 mm increment, and compared with the reference model. Fig. 10 shows that the stress decreases in a nonlinear behavior as the depth increases. All tensile and compressive stresses exceed the yield strength of the material (355 MPa) for corrugated depths less than 275 mm. The variation in deflection is relatively low for 100 mm panel depth and above, while a sudden increase in deflection is observed at 50 mm depth. Similar behavior occurs in the

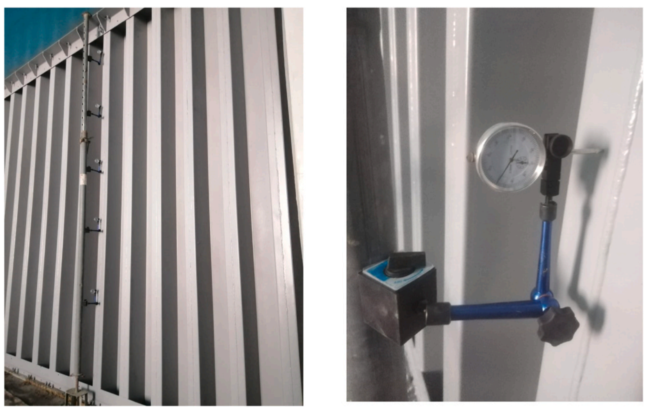

(a) (b)

Fig. 7. Displacement measurements for the steel tank (a) whole view and (b) close view of the dial gage.

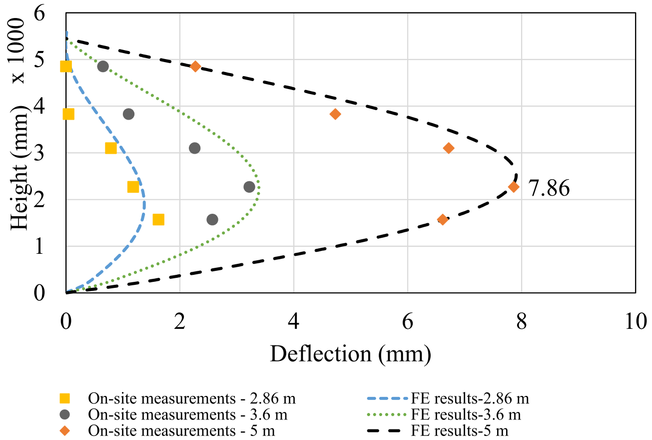

Fig. 8. Displacement of the on-site measurements versus F.E. results.

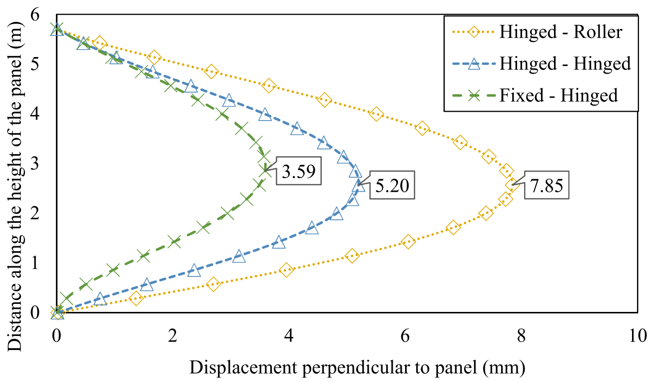

Fig. 9. Displacement of the panel for different BCs.

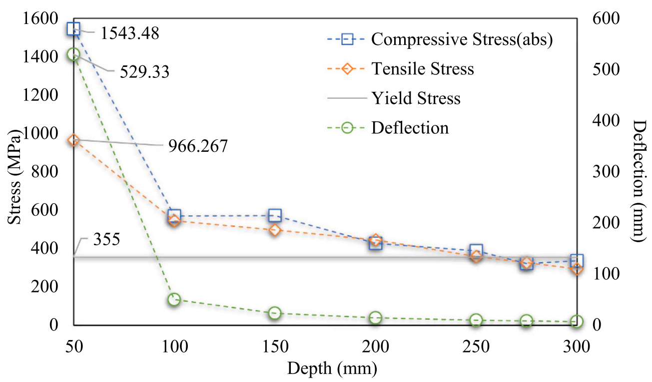

Fig. 10. Maximum stresses and deflection versus corrugated panel depth.

compressive stress at 50 mm depth, which indicates that the panel undergoes warping when the depth is below 100 mm for the current configuration.

3.6.3. *Thickness*

The effect of the thickness of the corrugated panel is studied from 2 mm to 7 mm thick with increment of 1 mm. Fig. 11 shows that both maximum tensile and compressive stress decrease with the increase of the panel thickness. The 5 mm thickness reports stresses below the yield stress (355 MPa), while lower thicknesses have higher stresses. A similar relationship is noticed for deflection variation with thickness.

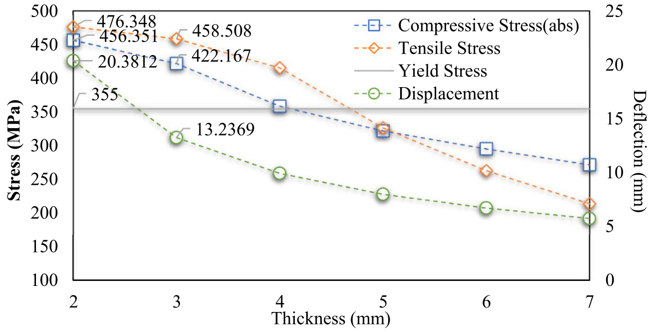

Fig. 11. Maximum stress and deflection versus corrugated panel thickness.

3.6.4. Trough to crest width ratio

The effect of the trough (water side) to crest (air side) width ratio is studied by increasing the trough width from 140 mm to 280 mm while fixing the crest width, which corresponds to the trough-to-crest width ratio varying from 1 to 2. Fig. 12 reports that the maximum stress on the crest side increases slightly with the increase of the trough/crest width ratio, with a maximum increase of 12 %. However, both compressive and tensile stresses are below the yield stress limit. It can be noted that the variation in the trough width for constant crest width has a limited effect on the overall stress and deflection.

3.6.5. Corrugation angle

The effect of corrugation angle is studied through variation of depth at a fixed angle. The angle is varied at 4 degrees increment from 78 degrees to 90 degrees. Fig. 13 reports the compressive stress at different angles and depths. It can be noted that the variation in angle has limited effect on the compressive stress, while the depth has a similar effect as previously reported in Section 3.6.2. The results show that angles over 86 degrees are required for this model with a depth of not less than 275 mm.

3.7. Diaphragm action of water tank

The diaphragm action of the panel is studied by applying a transverse displacement on the top of the panel in the *x*-direction. Fig. 14 shows stress concentration at the corners of the panel's crest. The stress concentration is because the first crest at the unrestrained corner carries most of the transverse load until it reaches the plastic stage. It can be noticed that the lower part, which is restrained by the angles and plates, has lower stress; while above the plates, the panel shows the highest stress concentration. This figure also shows that the stiffness of the panel is significantly influenced by the stiffness of the first pitch.

Fig. 15 and Table 1 show the hydrostatic pressure's effect on the stiffness of the restrained panel. The panel follows a linear behavior until warping due to compression stress occurs at the lower unrestrained part of the panel. It shows that hydrostatic pressure can decrease the panel stiffness towards the diaphragm action by around 7 % for the 5 mm thick panel. The drop in load capacity at failure load is only around 1 %. Therefore, the contribution of hydrostatic pressure is small due to the large thickness and stiffer end restraints by placing stiffened angles and plates at the end of the panel.

Water level is varied along the height of the panel with values 0, 2500, 3600, and 5000 mm, while transverse displacement is varied with values 0, 5, 10, 15, and 30 mm at the top of the panel. Fig. 16 shows the combined effect of hydrostatic pressure and transverse displacement. There is a clear threshold for transverse displacement at 15 mm, after which the increase in the maximum stress becomes small; however, for hydrostatic pressure, there is a gradual increase of loading for additional water level until the maximum allowable water level is achieved. This can be explained through the redistribution of forces along other parts of the panel after reaching the yield stress.

The effect of the thickness, end restraints on the diaphragm action without hydrostatic pressure is presented in Table 2. Thickness is

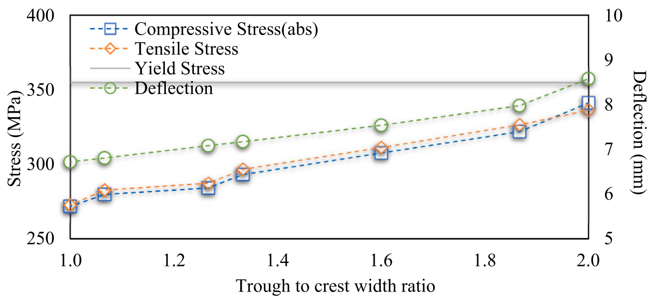

Fig. 12. Maximum stress and deflection versus trough/crest width ratio.

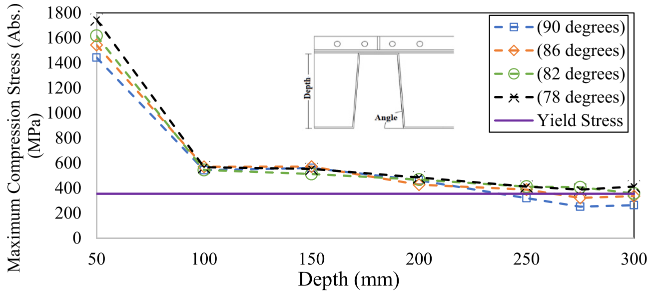

Fig. 13. Maximum compression results for different angle values versus panel depth.

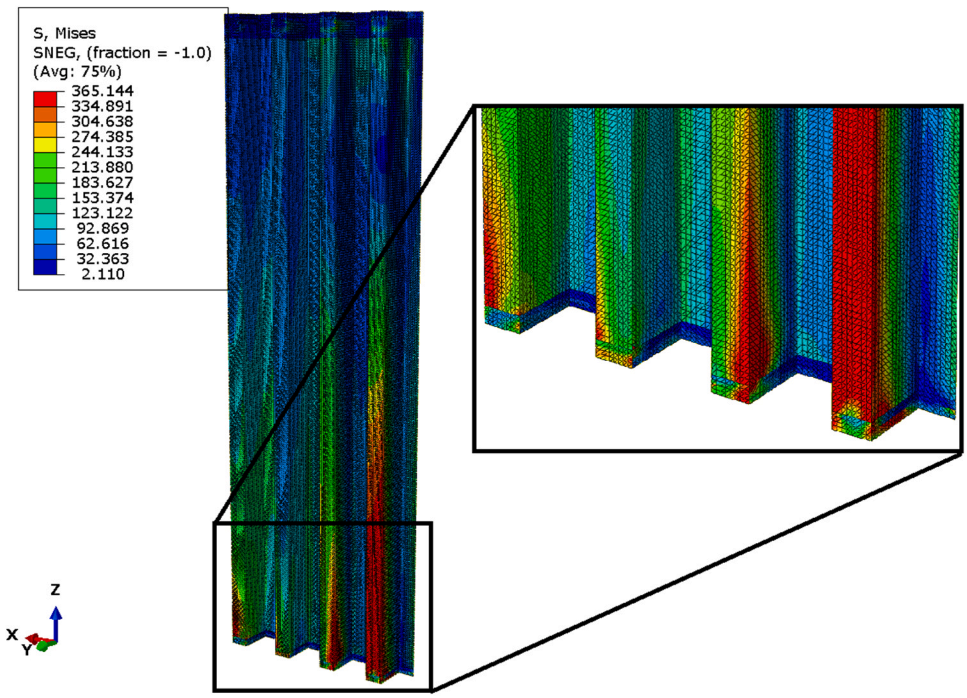

Fig. 14. Von-Mises Stress for combined hydrostatic pressure (5 m) and transverse displacement of 30 mm at the top.

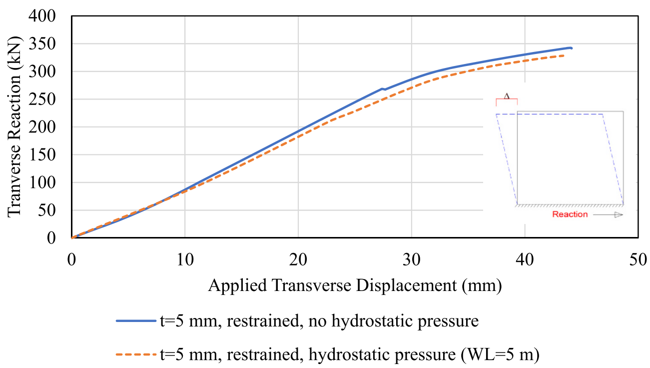

Fig. 15. Load displacement of the panel with and without hydrostatic pressure (Water level (WL) is 5000 mm) for restraint panel.

Table 1
Combined load effect on the stiffness of the panel.

Stiffness (kN/mm)			
Panel Thickness	Applied hydrostatic pressure (WL= 5 m)	No hydrostatic pressure applied	Difference %
3	5.13	5.84	12 %
5	9.09	9.80	7 %
8	12.90	14.31	10 %
10	16.16	17.62	8 %

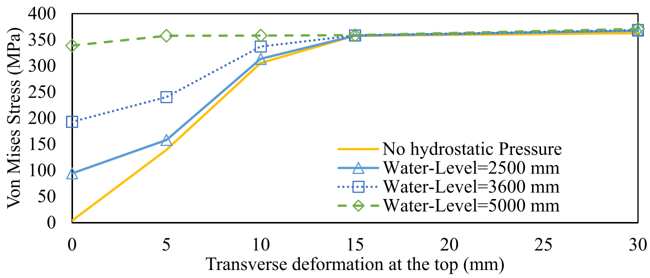

Fig. 16. Maximum Von-Mises Stress for combined hydrostatic pressure and diaphragm action for restraint panel.

Table 2
Effect of end restraints on the stiffness of the panel (No hydrostatic pressure applied).

Stiffness (kN/mm)			Stiffness Drop %
Panel Depth (mm)	275		
Thickness (mm)	Unrestrained Panel	Restrained Panel	
0.5	0.0087	1.165	99 %
1	0.05	2.08	98 %
5	2.42	9.32	74 %
10	8.03	17.62	54 %

varied with values of 0.5, 1, 5, and 10 mm. Stiffness of the panel is calculated with these parameters in the case of restrained and unrestrained panels. The drop in stiffness increases with smaller thicknesses, which shows that larger thickness can ultimately replace the end restraints, while the applicability of such large thickness might need further investigation.

The unrestraint panel is further studied by studying the effect of applied hydrostatic pressure at the water level (WL) of 5 m at two different thicknesses (5 and 10 mm), as shown in Fig. 17. While 10 mm thickness experiences higher load capacity than 5 mm, both thicknesses have similar effects in terms of combined loading. A drop in load capacity is observed at point A, where the panel undergoes a warping due to mixed loading; however, in the case of transverse load only, warping occurs much later at point B. The deformed shape at point A of the two panels with and without hydrostatic pressure verify this finding, as shown in Fig. 18. The drop in load capacity at the ultimate load is around 40 % and 5 % for 5 mm and 10 mm thick panels, respectively. Therefore, larger thicknesses can undergo similar behavior with and without hydrostatic pressure due to the limited effect of warping, while hydrostatic pressure

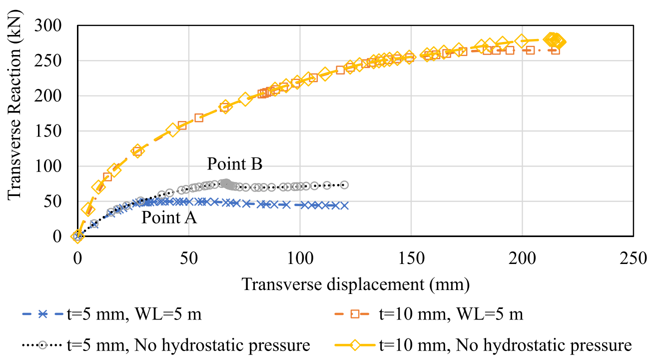

Fig. 17. Effect of combined hydrostatic pressure and transverse displacement for unrestrained panel.

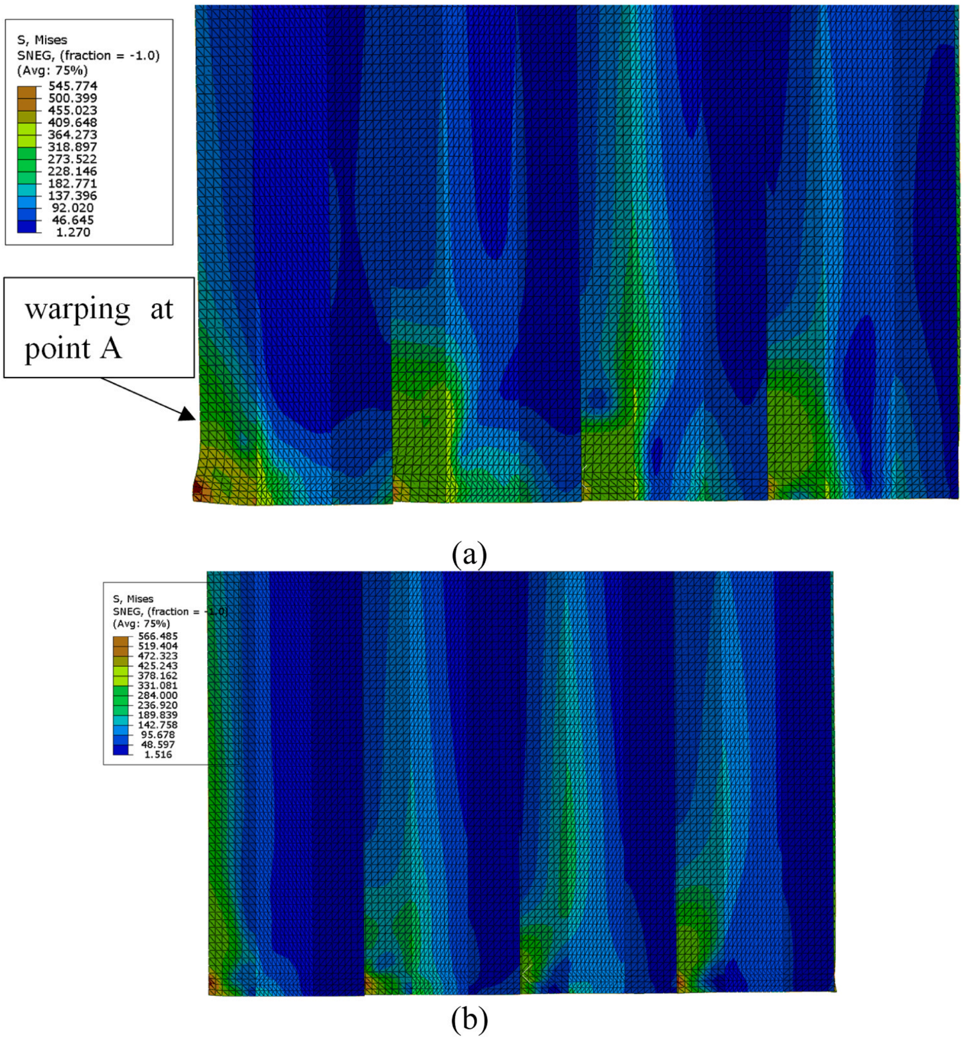

Fig. 18. Deformed shape of unrestraint panel subjected to (a) combined loading, (b) transverse load only.

has a significant effect on smaller thickness in unrestrained cases.

4. Full-scale implementation

The building selected for implementation is a hotel in Mecca, Saudi Arabia. It was initially designed to accommodate a concrete

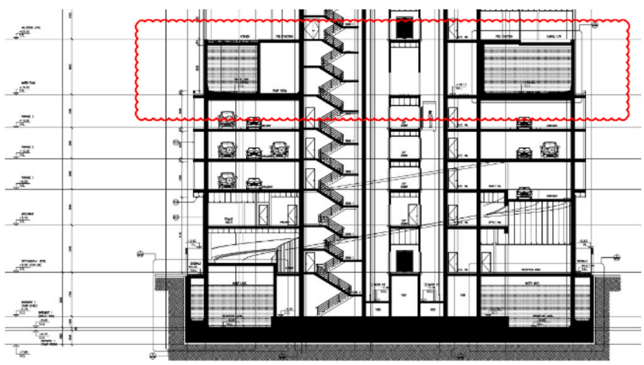

Fig. 19. Building layout - steel tank location is shown in the red cloud.

water tank. However, the scope has been changed to a structural steel tank due to time constraints.

The tank structure is composed of two water tanks on the fifth floor of each building lying between two concrete slabs at the levels of +19.20 m and +25.20 m, as shown in Fig. 19. Each building consists of 30 floors. The tank is installed on a concrete slab of 60 cm thick. The concrete strength of 40 MPa is at a level of (+19.20), and the roof of the tank is the upper concrete slab at level (+25.20). The upper concrete slab is a prestressed slab of the uncracked section with a thickness of 35 cm and concrete strength of 35 MPa. The lower slab is designed to support the required storage quantity, but using reinforced concrete tank. Due to tight project schedule, a solution was provided to use irregular steel tanks rather than reinforced concrete (RC) tanks. Using steel tanks will save about 90 % of the RC's dead load. The lower concrete slab is painted with cementitious waterproofing paint to prevent water from reaching steel reinforcement in case of any leakage. The upper slab is painted with epoxy paint to resist evaporated water from harming the upper prestressed slab.

The tank shape follows the existing floor layout, including many obstacles in the floor, such as columns, core walls, shear walls, stairs, elevators, duct openings, and pump room, as shown in Fig. 20. The steel tanks consist of corrugated wall panels, flat floor plates, top and bottom steel stiffened angles, anchors to fix the angles to floor and roof concrete slabs, anchor bolts for connecting the wall panels to angles during assembly, and steel plates for casing internal concrete columns existing inside tank.

4.1. Materials

Corrugated panel, plates, angles, and stiffeners are manufactured using steel grade 50, where the stress-strain curve is shown in Fig. 5. Anchor bolts' types and sizes are shown in Table 3. The anchor bolts used in the upper slab are 16 mm diameter with an effective anchorage depth of 85 mm, and the lower anchor bolts are 20 mm diameter with an effective anchorage depth of 101 mm. For welding, Esab welding rod is used of type: E71T-1 C as per SFA/AWS A5.20 with a thickness of 1.2 mm and C1 shielding gas.

4.2. Fabrication

Plates are cut to length according to cutting lists using a plasma cutting machine for 10 mm thick plates and the hydraulic shearing machine for thinner plates. Steel plates are bent to reach the required corrugated profile for one pitch (i.e., one crest and two troughs). Every four pitches are welded together to form one panel. Special care is taken to ensure the exact dimensions, which starts by adjusting the single unit dimensions in the start, middle, and end, then adjusting the spacing between single units, and finally assembling several units together by tack welding, as shown in Fig. 21.

After the fitting, the panels are welded using CO_2 electric welding machines. Automatic robotic welding carriages are adapted and programmed to apply full welding for longitudinal lines in panels while minimizing defects and increasing productivity, as shown in Fig. 22. The adapted machines weld two longitudinal lines at the same time. Other parts, such as stiffeners, angles, and plates, are welded manually. The panels are handled using a vacuum lifting machine, as shown in Fig. 23, to ensure proper and safe handling of the panel without damage. This vacuum machine is manufactured specifically for the panel weight and dimension, which includes different directions of motion and 180 degrees of rotation to facilitate panel handling and erection.

The steel surface is subjected to Sa 2½ blast-cleaning according to ISO 8501–1:2007, then painted to both air and water sides, as shown in Fig. 24, following the paint specifications mentioned in Table 4. Special care is given when choosing water-side paints suitable for potable water.

4.3. Material handling and erection

Panels are delivered to site and stored properly until erection. The installation process starts with fixing the anchors and supporting angles, as shown in Fig. 25.

4.3.1. Panels handling, assembly and welding

Panels are transported and lifted to tank floor level using mobile and tower cranes, as shown in Fig. 26. After lifting panel to the tank level, it is handled by a forklift with attached custom-built magnetic lift, which is designed and fabricated according to the panels size shown in Fig. 27. Panels are fixed in their positions and connected to thetop and bottom angles using bolts, washers and nuts, as shown in Fig. 28. Panels are assembled with the adjacent ones using temporary welds first, and then vertical continuous welding lines are preformed using automatic magnetic welding trucks, as shown in Fig. 29. Welding performed from inside and outside using three welding passes: root pass, top pass from inside, and top pass from outside. Other welds for base and top head plates of panels are welded using manual welding by welders.

Inner concrete columns inside tank are cladded with steel plates and welded together to prevent any leakage from columns. The columns are painted with cementitious waterproof paint, and then plates are directly cladded on it without corrugation. The tanks' supply inlets, outlets, overflow, cleaning drain and stainless-steel stair are welded and tested in their locations according to mechanical drawings.

4.3.2. Floor sheets assembly

After vertical panel installation, steel backing plates with a width of 15 cm are placed on the ground along each plate welding line, as shown in Fig. 30(a). Floor plates are laid on the backing plates and fitted together using tack welds. The floor plates are also welded with the lower end plate of vertical panels, as shown in Fig. 30(b) and (c).

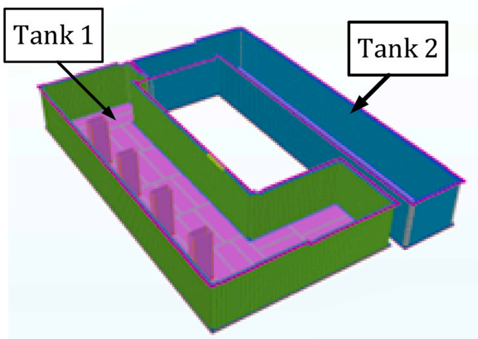

Fig. 20. Floor tank layout showing two adjacent tanks.

Table 3
Anchor bolt specifications.

item	Description	Lower Anchor bolt	Upper Anchor bolt
1	Anchor type and size	Hilti HST3 M20 hef2	Hilti HST3 M16 hef2
2	Gap filling	Hilti Seismic Set M20	Hilti Seismic Set M16
3	Effective Anchorage depth	101 mm	85 mm

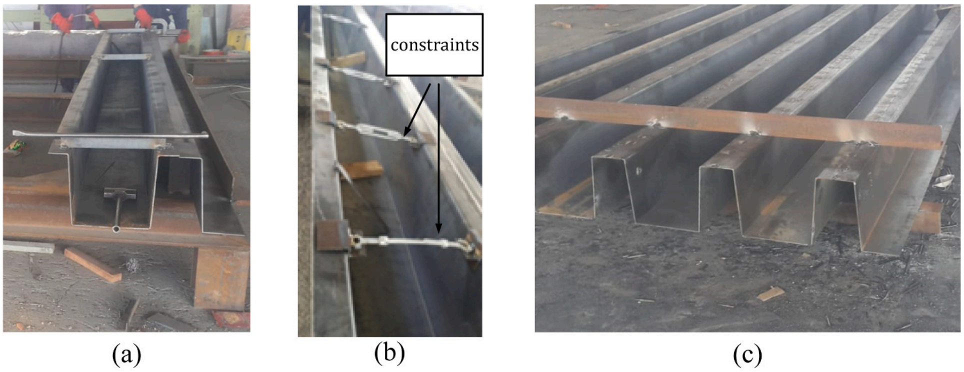

Fig. 21. Fitting and assembly of panels (a) adjusting the single unit dimensions in the start, middle, and end, (b) adjusting the single unit at a unit spacing, (c) Assembly of several panels together.

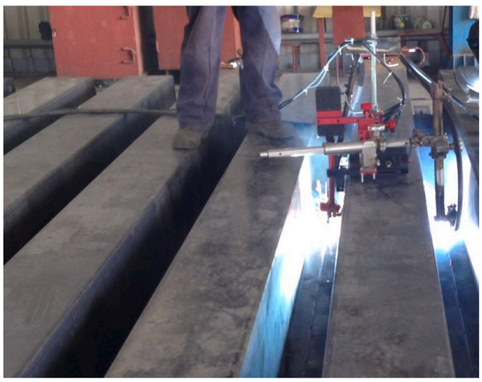

Fig. 22. Corrugated panel during and after welding.

Fig. 23. Specially manufactured vacuum lift machine for panels handling.

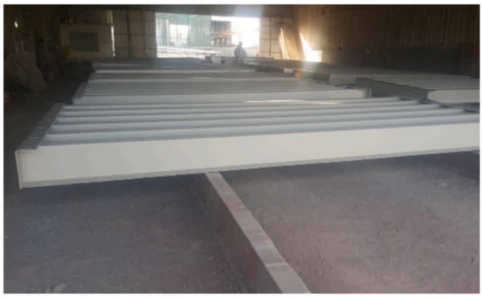

Fig. 24. Panel after painting in factory.

Table 4
Paint specifications applied on workshop and site.

Factory		Site	
Air side	Water side	Air Side	Water side
Penguard Express, Grey, Fig. (13) 100 microns	Penguard Express, Red, Fig. (14) 100 microns	Hardtop Xp, Grey 100 microns	Tankguard 412, White 200 microns

4.3.3. Testing of welded joints

Along welding process, testing is performed on vertical and horizontal welds. Liquid penetration and magnetic particle tests are done on all joints from inside and outside to ensure welding quality, as shown in Fig. 31(a). Vacuum test is done on floor and column joints to ensure that there is no leakage, as shown in Fig. 31(b). Then all tank panels are closed, welded with floor plates, and tested where the only access to tank inner space is through the tank opening in the tank roof slab.

4.3.4. Painting

Tank is carefully cleaned, and joints are grinded. Then the unpainted areas along welded joints are painted using epoxy primer up to the thickness delivered from factory from inside and outside. The whole tank is painted with final coating to the full required thickness as shown in Fig. 32. Painting thicknesses are measured continuously during painting.

4.3.5. Water leakage testing

Finally, after painting passes its curing duration, the tank is filled to the maximum level to perform a full water leakage test, as shown in Fig. 33. Leakage check is done through two steps: (1) Placing sign at water level and checking the water level at every defined period. (2) Moving around tank and observing if any leakage occurs from wall panels or on the floor. The presence of air space around the tanks enhances the water temperature inside the tank. Water temperature in the tank is moderate (around 20 °C) in very high temperature days (48–50 °C), which saves much the thermal insulation costs required for similar tanks on roof in this arid high

(a) (b)

Fig. 25. Fixation of (a) upper and (b) lower anchors.

Fig. 26. Outer view for the building showing the tank position and handling of the panel.

temperature zones.

5. Discussions

Previous results show that boundary conditions and corrugated depth have a significant effect on the panel, while thickness, trough-to-crest width ratio, and pitch angle have a slight effect on the panel. Therefore, attention should be paid to corrugation depth and panel thickness. Further analysis is carried out on the combined effect of the hydrostatic pressure and transverse displacement. The proposed end restraints can help reduce the distortion of the panel and increase its stiffness by almost three times, achieving 9.32 kN/mm compared to 2.42 kN/mm for the unrestrained panel in case of the 5 mm thick panel. At the same time, the 5 mm thick panel has a three order of magnitude of stiffness compared to the 0.5 mm thick panel.

(a) (b)

Fig. 27. (a) Custom built magnetic lift, (b) Handling panel at tank level using custom lift.

Fig. 28. Fixation and assembly of panels on-site.

Combined loading shows that the panel with 275 mm depth and 5 mm thickness acts in the elastic range for full hydrostatic pressure and transverse displacement up to 15 mm. Transverse displacement of more than 15 mm forces the panel to redistribute its stress along other pitches until warping failure. Results show that the effect of the hydrostatic pressure reduces when the panel has stiffer end restraints or high panel thickness.

The stress state of the corrugated panel differs with the loading conditions, as shown in Fig. 34. Based on the analysis, stresses are mainly in z-direction, where σ_x and τ_{xz} can be neglected. The hydrostatic pressure is mainly resisted by the corrugation depth, yielding tensile stress at the crests and compressive stress at the troughs. It should be noted that the stress is the maximum at 1/3 water height. The transverse loading acting in the right direction leads to compressive stress at the lower part of the right pitch (i.e. trough and crest) and tensile stress at the lower part of left pitch. For combined loading, the right trough is subjected to combined compressive stress due

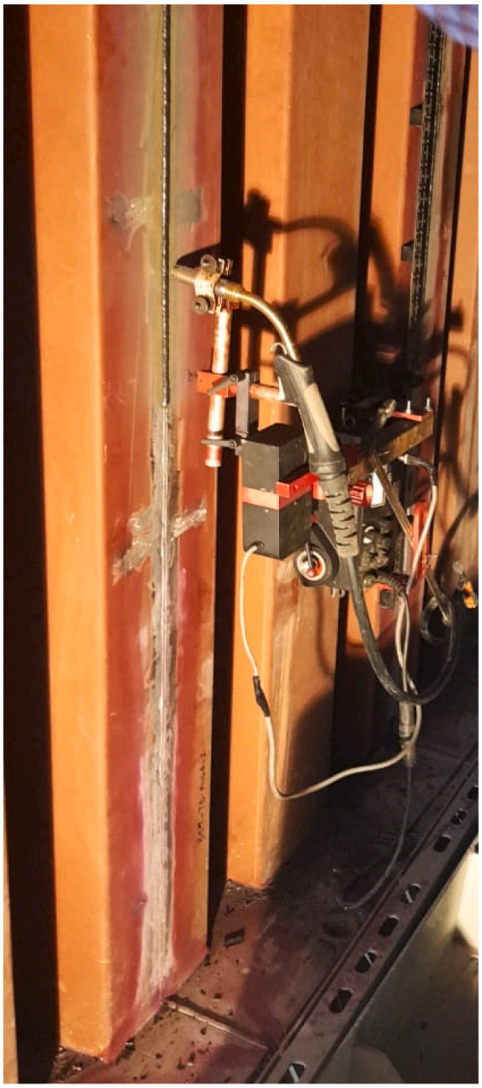

Fig. 29. Automatic robotic welding of wall joints.

(a) (b) (c)

Fig. 30. Floor sheet assembly (a) handling of floor plates, (b) welding of floor plates (c) welded plates profile.

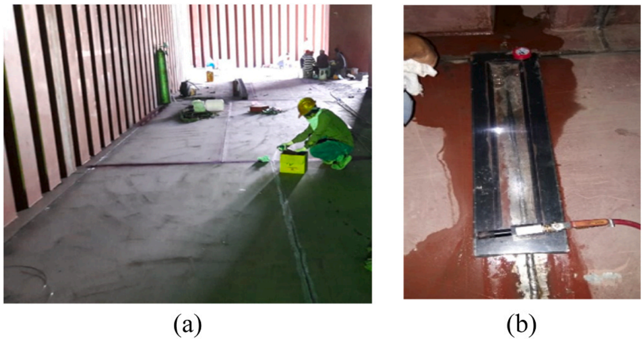

Fig. 31. Testing of welded joints using (a)DPT and (b) Vacuum box.

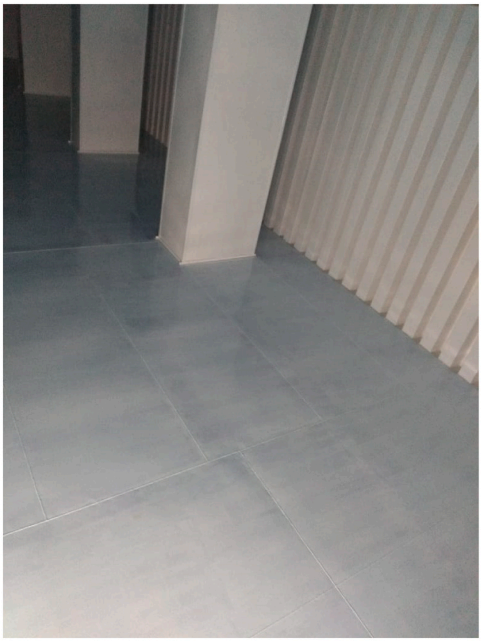

Fig. 32. Final on-site painting.

to hydrostatic pressure and transverse loading. Designers are encouraged to check if the combined stress is still lower than those from the sheet warping failure.

Based on the FE results, panels are manufactured and deployed on-site, where real-time measurements confirm the FE model results. Cold bending of a relatively larger thickness (i.e., 5 mm) into corrugated panel than conventional corrugated sheets (i.e., 0.5–2 mm) achieve higher stiffness against the diaphragm and hydrostatic loads.

Limitations and potential challenges in implementing the proposed system include: (1) buckling analysis is required in case the vertical movement of the tank is restrained; (2) structural resilience for seismic activity should be considered when it is used in high seismic region; and (3) sloshing effect due to seismic load should be considered when it is used in low seismic region.

6. Conclusions

In this study, a proposed corrugated sheet tank is evaluated against combined hydrostatic pressure and diaphragm action. An FE model is created, validated using the full-scale fabricated model, and used to carry out a parametric study to study the effects of boundary conditions, corrugated depth, sheet thickness, trough-to-crest width ratio, and inclination angle of the corrugation. Based on the parametric study, reference dimensions are recommended, and further analysis is carried out to study the diaphragm action of the panel. Finally, the implementation of the full-scale steel tank is presented. It can be concluded that:

1. Using of paneled steel tanks can be an efficient solution for water storage inside buildings. Compared with reinforced concrete tanks, it can save time and cost and decrease structural loads.

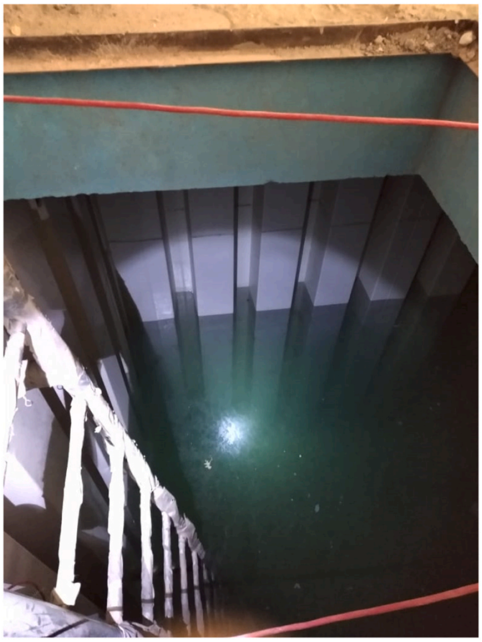

Fig. 33. Water leakage testing.

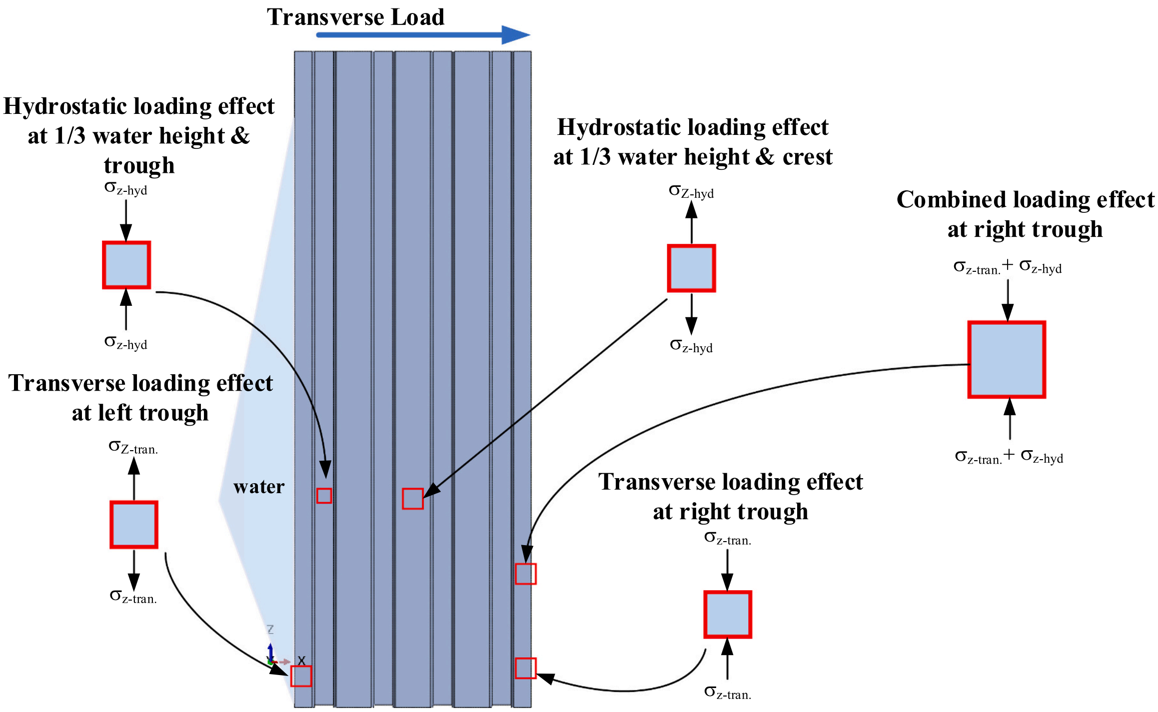

Fig. 34. Stress state at hydrostatic pressure, transverse and combined loadings.

2. Corrugated steel wall panels can be used to install irregular panel shapes according to the building architecture, increasing the water storage quantity.
3. Both boundary conditions and corrugated depth have a significant effect on the displacement of the panel. The corrugated depth that meets the yield stress is more than 275 mm.
4. Thickness varies inversely proportional to tensile and compressive stress and deflection. A 5 mm thickness reports 326 MPa stress, which is lower than yield stress (355 MPa).

5. Trough-to-crest ratio and angle of corrugation have limited effect on the panel stresses.
6. In case of restrained panel, the stiffness of the first pitch determines the stiffness of the whole panel, as stress is mainly carried by the first pitch during the elastic analysis.
7. Recommended configuration allows the panel to undergo elastic stresses for the full height of hydrostatic pressure, in addition to transverse loads up to 15 mm. Transverse loads of more than 15 mm will cause plastic stress, where the panel redistributes the stress until failure.
8. Failure of the restrained panel, which is warping in the sheets, occurs at the lower area above the location of the lower angles. Therefore, it is recommended to increase the sheet thickness to avoid such failure.
9. Failure occurs due to combined compressive stresses from hydrostatic pressure and transverse loading. Designers are advised to check that the induced combined stresses are less than those from the sheet warping failure.
10. The hydrostatic pressure has a higher contribution towards decreasing the transverse stiffness and load capacity of the panel at smaller thickness and unrestrained conditions.

Future work includes sloshing effects, lifetime of the paint and durability of steel, the effect of steel grade, intermediate bulk weight on building seismic stability, and analysis of water chemistry.

CRediT authorship contribution statement

Mohamed Elsayad: Formal analysis, Methodology, Writing – original draft, Writing – review & editing. **Mostafa Yossef:** Conceptualization, Methodology, Validation, Writing – original draft, Writing – review & editing. **An Chen:** Methodology, Writing – original draft, Writing – review & editing. **Mohamed Abdel-Latif Youssef:** Conceptualization, Writing – review & editing, Data curation, Methodology, Project administration, Resources, Supervision, Writing – original draft.

Declaration of Competing Interest

The authors declare that they have no known competing financial interests or personal relationships that could have appeared to influence the work reported in this paper.

Data availability

Data will be made available on request.

Acknowledgements

The authors would like to thank Engineering Construction Company (ECE), Al-Arif Company, and Zakher group for facilitating on-site measurements and full-scale implementation. Mostafa Yossef would like to thank the Research Council of Finland (Academy of Finland) for the postdoctoral fellowship grant no. 348611.

References

[1] J. Qiu, Q. Zhao, C. Yu, Z. Wang, Lateral behavior of trapezoidally corrugated wall plates in steel plate shear walls, Part 2: shear strength and post-peak behavior, Thin Walled Struct. 174 (2022) 109103, https://doi.org/10.1016/J.TWS.2022.109103.
[2] J.Z. Tong, Y.L. Guo, Elastic buckling behavior of steel trapezoidal corrugated shear walls with vertical stiffeners, Thin Walled Struct. 95 (2015) 31–39, https://doi.org/10.1016/J.TWS.2015.06.005.
[3] N. Usefi, P. Sharafi, H. Ronagh, Numerical models for lateral behaviour analysis of cold-formed steel framed walls: state of the art, evaluation and challenges, Thin Walled Struct. 138 (2019) 252–285, https://doi.org/10.1016/J.TWS.2019.02.019.
[4] Z. Nagy, B. Bács, A. Kelemen, A. Sánduly, Ö. Nagy, B. Lőrincz, Rafter-purlin connection stiffness impact on the stress skin effect of corrugated sheet claddings, Thin Walled Struct. 185 (2023) 110615, https://doi.org/10.1016/j.tws.2023.110615.
[5] A. Chen, Y. Zhang, H. Wu, A multifunctional reinforced concrete tuned liquid wall damper with optimal design variables, Pract. Period. Struct. Des. Constr. 28 (1) (2023), https://doi.org/10.1061/PPSCFX.SCENG-1195.
[6] M. Manga, et al., The effect of household storage tanks/vessels and user practices on the quality of water: a systematic review of literature, Environ. Syst. Res. 10 (1) (2021), https://doi.org/10.1186/S40068-021-00221-9.
[7] K.R.F. De Oliveira, P. Cheung, W. Uhl, I. Slavik, K.R. Oliveira, P.B. Cheung, Water quality aspects related to domestic drinking water storage tanks and consideration in current standards and guidelines throughout the world–a review, J. Water Health (2020), https://doi.org/10.2166/wh.2020.052.
[8] M.E. Dusalimov, I.R. Karimov, I.I. Khasanov, E.S. Gaysin, Y.A. Frolov, and O.A. Nasibullina, Estimate Tank Quality Margin. iopscience.iop.org, doi: 10.1088/1755-1315/459/3/032055.
[9] T. Yingsamphancharoen, K. Piriyakul, Feasibility study of steel reinforcement of polyethylene corrugated horizontal pipe for on-site underground water storage tanks and their applications, Case Stud. Constr. Mater. 17 (2022) e01578, https://doi.org/10.1016/J.CSCM.2022.E01578.
[10] T.A. El-Sayed, Y.B. Shaheen, F.H. Mohamed, R.M. Abdelnaby, Performance of ferrocement composites circular tanks as a new approach for RC tanks, Case Stud. Constr. Mater. 19 (2023) e02228, https://doi.org/10.1016/J.CSCM.2023.E02228.
[11] T. Tursunkululy, et al., Analysis of strength and eigenfrequencies of a steel vertical cylindrical tank without liquid, reinforced by a plain composite thread, Case Stud. Constr. Mater. 18 (2023) e02019, https://doi.org/10.1016/J.CSCM.2023.E02019.
[12] M.E. Zayed, et al., Applications of cascaded phase change materials in solar water collector storage tanks: a review, Sol. Energy Mater. Sol. Cells 199 (2019) 24–49, https://doi.org/10.1016/J.SOLMAT.2019.04.018.
[13] Y.P. Chandra, T. Matuska, Stratification analysis of domestic hot water storage tanks: a comprehensive review, Energy Build. 187 (2019) 110–131, https://doi.org/10.1016/J.ENBUILD.2019.01.052.

[14] K. Magnucki, P. Stasiewicz, Critical sizes of ground and underground horizontal cylindrical tanks, Thin-Walled Struct. 41 (4) (2003) 317–327, https://doi.org/10.1016/S0263-8231(02)00097-6.
[15] M.S. Kim, J.H. Kim, S.K. Kim, and J.M. Lee, Experimental Investigation of Structural Response of Corrugated Steel Sheet Subjected to Repeated Impact Loading: Performance of LNG Cargo Containment System, Applied Sciences 2019, 9(8) 1558, 2019, doi: 10.3390/APP9081558.
[16] C.H. Roy and M. Mudlock, Seismic analysis and design of a 21,000-gallon frac tank considering the fluid-structure interaction effects for a FLEX response at a nuclear power station, in: Proceedings of the Structures Congress 2017: Buildings and Special Structures - Selected Papers from the Structures Congress 2017, 758–771, 2017, doi: 10.1061/9780784480410.063.
[17] S.E.A. Hosseini, S. Beskhyroun, Fluid storage tanks: a review on dynamic behaviour modelling, seismic energy-dissipating devices, structural control, and structural health monitoring techniques, Structures 49 (2023) 537–556, https://doi.org/10.1016/j.istruc.2023.01.146.
[18] M.Z. Kangda, An approach to finite element modeling of liquid storage tanks in ANSYS: a review, Innov. Infrastruct. Solut. 6 (4) (2021), https://doi.org/10.1007/S41062-021-00589-8.
[19] R.C. Jaca, L.A. Godoy, Wind buckling of metal tanks during their construction, Thin Walled Struct. 48 (6) (2010) 453–459, https://doi.org/10.1016/J.TWS.2010.01.001.
[20] S. Miladi, M. S. Razzaghi, Failure analysis of an un-anchored steel oil tank damaged during the Silakhor earthquake of 2006 in Iran, Eng. Fail Anal. 96 (2019) 31–43, https://doi.org/10.1016/j.engfailanal.2018.09.031.
[21] A.M. Teamah *et al.*, Mass and Heat Transfer at A Corrugated Wall of A Square Stirred Tank Reactor and Possible Applications. ⟨https://doi.org/10.1080/08916152.2022.2162165⟩, 2022, doi: 10.1080/08916152.2022.2162165.
[22] S.M. Ghodratian-Kashan, S. Maleki, Experimental investigation of double corrugated steel plate shear walls, J. Constr. Steel Res. 190 (2022), https://doi.org/10.1016/j.jcsr.2022.107138.
[23] S. Jin, Q. Wang, J. Zhou, J. Bai, Experimental and numerical investigation of assembled multi-grid corrugated steel plate shear walls, Eng. Struct. 251 (2022), https://doi.org/10.1016/j.engstruct.2021.113544.
[24] R.M. Wu, L.Q. Wang, J.Z. Tong, G.S. Tong, W. Gao, Elastic buckling formulas of multi-stiffened corrugated steel plate shear walls, Eng. Struct. 300 (2024), https://doi.org/10.1016/j.engstruct.2023.117218.
[25] B. Zhang, J. Yu, W. Chen, H. Wang, J. Xu, Stress states and shear failure mechanisms of girders with corrugated steel webs, Thin Walled Struct. 157 (2020), https://doi.org/10.1016/j.tws.2020.106858.
[26] W. Wang, Q. Luo, Z. Sun, B. Wang, S. Xu, Relation analysis between out-of-plane and in-plane failure of corrugated steel plate shear wall, Structures 29 (2021) 1522–1536, https://doi.org/10.1016/j.istruc.2020.12.030.
[27] X. Zhang, J. Sun, R. Wu, Y. Peng, Buckling performance of inner corrugated pressure shells under external hydrostatic pressure, Ocean Eng. 288 (2023), https://doi.org/10.1016/j.oceaneng.2023.115963.
[28] N.M. Yossef, A new approach to estimate the shear strength of curved corrugated steel webs, Structures 24 (2020) 400–414, https://doi.org/10.1016/j.istruc.2020.01.028.
[29] L.L. Wu, L.P. An, Y. Bai, In-plane stability of steel circular closed supports with I-section of sinusoidal corrugated webs: experimental and numerical study, Tunn. Undergr. Space Technol. 106 (2020), https://doi.org/10.1016/j.tust.2020.103566.
[30] K. Liu, S. Zong, Y. Li, Z. Wang, Z. Hu, Z. Wang, Structural response of the U-type corrugated core sandwich panel used in ship structures under the lateral quasi-static compression load, Mar. Struct. 84 (2022), https://doi.org/10.1016/j.marstruc.2022.103198.
[31] E.R. Bryan, W.M. EL-Dakhakhni, Behaviour of sheeted portal frame sheds: theory and experiments, Proc. Inst. Civ. Eng. 29 (4) (1964) 743–778, https://doi.org/10.1680/iicep.1964.9593.
[32] M. Yossef, Ain Shams University, Behaviour and Strength of Diaphragms in Steel Structures, Ain Shams University (2013).
[33] J.M. Davies, M.J. Roberts, Y.C. Wang, Stressed skin theory and structure cladding interaction: safety concerns with Big Sheds, Thin Walled Struct. 169 (2021) 108415, https://doi.org/10.1016/j.tws.2021.108415.
[34] M. Youssef, A.M. Sanad, A. Salem, A.H. Badawy, Efficiency of corrugated sheets in resisting membrane forces, in: K. Jármai, J. Farkas (Eds.), Design, Fabrication and Economy of Metal Structures, Springer Berlin Heidelberg, Berlin, Heidelberg, 2013, pp. 171–177, https://doi.org/10.1007/978-3-642-36691-8.
[35] X. Yun, L. Gardner, Stress-strain curves for hot-rolled steels, J. Constr. Steel Res. 133 (2017) 36–46, https://doi.org/10.1016/j.jcsr.2017.01.024.
[36] A. Chen, M. Yossef, P. Hopkins, A comparative study of different methods to calculate degrees of composite action for insulated concrete sandwich panels, Eng. Struct. 212 (2020) 110423, https://doi.org/10.1016/j.engstruct.2020.110423.